Applied *Nanomaterials and smart Polymers,*
Online ISSN: 2981-0434
Vol. 2, No. 6

ANSP

Nanoparticle-Driven Rheological Reinforcement and Flame Retardancy in Multiple-Recycled PET Fibers

Karim Heydari [1,2], Ali Zadhoush [1], Ali Akbar Yousefi [2*]

[1] Department of Textile Engineering, Isfahan University of Technology (IUT), Isfahan, Iran
[2] Department of Plastics Engineering, Faculty of Polymer Processing, Iran Polymer and Petrochemical Engineering, P.O Box 14965/115 Tehran, Iran

*** Corresponding Author :** Ali Akbar Yousefi: a.yousefi@ippi.ac.ir

Abstract
The recycling of polyethylene terephthalate (PET) has become increasingly important due to environmental concerns and the growing demand for polyester fibers. However, multiple recycling cycles result in chain scission, reduced intrinsic viscosity, and deterioration of rheological and mechanical properties, limiting the reuse of recycled PET (rrPET) in high-performance applications. This study investigates a dual modification strategy combining reactive rheology with nanocomposite flame-retardant engineering to restore rrPET to fiber-grade quality. Epoxy-based chain extender Joncryl ADR4468 was employed to reconnect fragmented chains, increase molecular weight, and enhance melt elasticity. Rheological characterization confirmed significant improvements in complex viscosity, yield stress, and viscoelastic stability, enabling stable fiber spinning.
To address flammability, halogen-free zinc phosphinate (ZPi) and Cloisite 30B nanoclay were incorporated. The synergistic action of phosphorus-based flame retardant and layered silicate nanofillers improved thermal stability, enhanced shear-thinning behavior, and promoted uniform dispersion within the polymer matrix. Morphological analyses revealed homogeneous fiber structures with reduced agglomeration, while flame-retardant testing demonstrated elevated limiting oxygen index (LOI) values and compliance with UL94 standards.

Keywords:PET, fiber, rheology, chain extender, flame-retardant, recycling

1. Introduction

Recycling of polyethylene terephthalate (PET) has gained significant attention due to growing environmental concerns, yet the rheological challenges of processing multiple-recycled PET (rrPET) remain unresolved [1] [2] [3]. PET is widely used in packaging because of its excellent barrier properties against moisture, oxygen, and other gases, and beyond packaging it finds extensive applications in textile fibers, construction materials, and household products. However, its petroleum-based origin and resistance to biodegradation raise serious sustainability

issues. The increasing global demand for polyester fibers has sharply accelerated PET waste generation, particularly in the textile sector, underscoring the urgent need for effective recycling strategies that can restore both the rheological integrity and functional performance of rrPET [4].

Recycling PET offers a sustainable pathway to mitigate environmental impact. However, multiple recycling cycles lead to chain scission, reduction in intrinsic viscosity, and deterioration of mechanical and rheological properties, limiting rrPET's reuse in high-performance applications [5] [6] [7] [8]. The rheological challenges of rrPET include reduced melt strength, poor viscoelastic stability, and compromised spinnability [9]. These issues hinder its application in fiber spinning and advanced processing methods [10] [11] [12].

Reactive rheology has emerged as a promising approach to restore rrPET properties. By introducing multifunctional chain extenders (CEs), in-situ chemical modifications occur during processing, reconnecting fragmented chains and promoting long-chain branching [13] [14]. Epoxy-based chain extenders such as Joncryl ADR 4468 react with terminal carboxyl and hydroxyl groups in degraded PET chains. These reactions increase molecular weight, enhance intrinsic viscosity, and improve melt elasticity, thereby restoring fiber-grade processability [15] [16] [17].

Mechanistic frameworks such as Boltzmann superposition, Mooney–Rivlin modeling [18], and Arrhenius evaluation [19] provide a coherent understanding of how chain extension reactions translate into macroscopic viscoelastic reinforcement and improved thermal stability [20].

Beyond rheological recovery, rrPET fibers must meet safety requirements. Polyester fibers are inherently flammable, producing rapid flame propagation and toxic gases upon ignition, which critically reduce evacuation time during fire incidents [21] [22] [23] [24]. Halogen-free flame retardants such as zinc phosphinate (ZPi) [25] have emerged as effective alternatives, offering strong flame inhibition while minimizing toxic emissions. Nanoclays like Cloisite 30B further enhance thermal stability and mechanical flexibility [26] [27] [28].

The synergistic incorporation of chain extenders, halogen-free flame retardants such as zinc phosphinate, and nanoclays like Cloisite 30B enables rrPET composites to achieve both structural recovery and enhanced flame resistance. The presence of nanoclays contributes to improved thermal stability, better dispersion of additives, and increased mechanical flexibility, while simultaneously reinforcing the flame-retardant action of phosphorus-based compounds [29] [30].

The novelty of this work lies in the dual integration of rheological reinforcement and flame-retardant nanocomposite engineering within recycled PET systems. Unlike conventional approaches that address either processability or safety in isolation, this study demonstrates how chain extension reactions synergize with halogen-free phosphorus additives and nanoclays to simultaneously restore molecular integrity, enhance viscoelastic stability, and improve fire resistance. This comprehensive strategy not only elevates rrPET to fiber-grade quality but also establishes a sustainable pathway for its industrial adoption in advanced textile applications, bridging the gap between environmental responsibility and high-performance material design.

The integration of rheological reinforcement with flame-retardant nanocomposites offers a holistic strategy for valorizing recycled PET. Through the synergistic action of chain extension reactions and halogen-free flame-retardant nanofillers such as zinc phosphinate and Cloisite 30B,

rrPET can simultaneously overcome fundamental processing limitations and meet critical safety requirements. This dual modification not only restores molecular integrity and viscoelastic stability but also enhances thermal resistance and mechanical flexibility, enabling the transformation of rrPET into a sustainable, high-performance material suitable for fiber spinning and advanced textile applications. Such synergy paves the way for industrial adoption of recycled PET in environmentally responsible sectors.

2. Experimental

2.1. Materials

Recycled rrPET, obtained from Life Gostar (a textile fiber recycling facility in Iran), was employed as the base polymer. The rrPET, supplied in powder form and derived from post-consumer textile fibers, exhibited an intrinsic viscosity (IV) of 0.375 ± 0.02 dL/g, reflecting significant degradation from previous processing cycles. To improve thermal and mechanical performance, Cloisite 30B (an organically modified montmorillonite, C30B) was incorporated, provided by BYK Additives, Germany. As a halogen-free flame retardant, Exolit OP 950 (ZPi nanoparticles) from Clariant, Germany was used. Additionally, ADR4468, a multifunctional epoxy-based chain extender with a molecular weight of 7250 g/mol, was supplied by BASF, Germany.

Prior to reactive processing, rrPET powder and ADR4468 were dried in a vacuum oven at 100°C for 4 h, while ADR was separately dried at 50°C for 4 h. After cooling to ambient temperature, the materials were blended with varying additive concentrations using a high-speed mixer to ensure homogeneous dispersion.

2.2. Processing and Sample Preparation

Reactive extrusion of rrPET blends was carried out using a co-rotating twin-screw extruder (ZSK25-WLE, W&P, Germany) equipped with a 25 mm screw diameter and an L/D ratio of 40. The recycled PET together with the modifiers was continuously introduced into the hopper at a controlled feed rate, while the screws operated at 250 rpm. A gradually increasing barrel temperature profile, ranging from 245°C to 270°C across six heating zones, ensured effective melt processing. The extrudate was shaped into filaments, quenched in a water bath, pelletized, and subsequently oven-dried. For fiber production, melt spinning was performed on a laboratory-scale spinning unit (CF Teck, Italy), with a progressive thermal gradient from 240°C at the hopper to 265°C at the nozzle. Polyester filaments were obtained under a roller take-up speed of 200 rpm and a fourfold draw ratio. All formulations incorporated chain extender ADR4468 at a fixed concentration to stabilize the molecular structure.

2.3. Characterization Methods

The rheological behavior of rrPET composites was investigated using an oscillatory rheometer (MCR 501, Anton Paar, Austria) equipped with a 20 mm parallel-plate geometry. Dynamic frequency sweep tests were performed at 265 °C, over an angular frequency range of 0.03–600 rad/s to evaluate viscoelastic properties and melt stability. Prior to each sweep, time-invariant viscosity was verified through pre-sweep time tests; when stability could not be confirmed, time-resolved SAOS measurements were conducted at 275 °C and $\omega = 100$ rad/s. In such cases, frequency-domain interpretations were limited to qualitative analysis without extrapolation to steady-state behavior.

Capillary rheology was measured using an automatic capillary viscometer (RHEOTEST LK2.2, Germany) in accordance with ASTM D3835, providing melt viscosity data at high shear rates. These results were compared with oscillatory shear data, and the Cox–Merz rule was applied solely as a compatibility check. Geometric and flow parameters, including pressure drop (ΔP), tube radius (R), length (L), and volumetric flow rate (Q), were used to calculate apparent wall shear stress, shear rate, and viscosity, with corrections applied for non-Newtonian flow behavior.

Intrinsic viscosity (IV) was determined in o-chlorophenol at 25 °C using an Ubbelohde viscometer. The viscosity-average molecular weight was estimated via the Mark–Houwink–Sakurada relation ($[\eta] = k \cdot M_n^{\alpha}$, with $k = 6.56 \times 10^{-4}$ and $\alpha = 0.73$), ensuring accurate correlation between chain conformation and molecular weight.

The cross-sectional morphology of polyester fibers was examined by scanning electron microscopy (SEM, Vega II XMU, Tescan, Czech Republic) after sputter-coating with a 30 nm gold layer to enhance conductivity. Imaging was performed under an accelerating voltage of 20 kV.

Thermal stability was assessed by thermogravimetric analysis (TGA, TA Instruments SDT Q600) under both air and nitrogen atmospheres, with a flow rate of 100 L/min and a heating rate of 10 °C/min from 20–800 °C. After reaching 800 °C, the inert atmosphere was replaced with air for 3 min to combust residual organics.

Flame-retardant properties were evaluated using the limiting oxygen index (LOI) method and vertical combustion tests according to UL-94 standards. Samples with dimensions of 130 × 13 × 3 mm were tested in both horizontal and vertical configurations.

3. Results and Discussion

3.1. Rheological Properties

As presented in Table 1, the incorporation of Joncryl ADR 4468 markedly enhances the rheological performance of recycled polyesters, thereby improving both fiber spinnability and molding behavior. The addition of up to 0.4 wt% chain extender leads to a noticeable rise in the complex viscosity of rPET, which can be attributed to increased cross-linking density, higher molecular weight, and a broader molecular weight distribution.

Table 1. Rheological properties of PET/CE blends at different compositions and shear rates (265°C)

Sample	PET (%)	CE (%)	η* (Pa· s)	η_{100}* (Pa· s)	η_{600}* (Pa· s)
CE0.0	100	0	23.2	26.8	27.1
CE020	99.8	0.2	38.6	39.9	40.4
CE040	99.6	0.4	57.9	47.0	40.4
CE060	99.4	0.6	56.8	48.3	48.7

The incorporation of a molecular weight increaser as a chain extender promotes shear-thinning behavior in recycled PET, shifting its response from Newtonian to non-Newtonian due to enhanced molecular entanglement within the branched architecture. This modification strengthens melt stability, viscoelastic performance, and overall processability, thereby improving fiber-spinning efficiency. Experimental results (Table 1) identified CE040 (0.4 wt% CE, 99.6 wt% PET) as the optimal formulation. Rheological characterization of this composition, conducted using both rotational and capillary rheometers, revealed consistent trends across methods, with outcomes further validated through established rheological models. This convergence underscores the accuracy and reliability of the applied techniques in assessing the rheological behavior of modified rrPET.

The rheological performance of rrPET and CE040 specimens was examined at 265 °C using both rotational and capillary rheometers. Frequency sweep analyses demonstrated elevated complex viscosities at low angular frequencies, which progressively declined with increasing frequency—characteristic of non-Newtonian, shear-thinning behavior. To describe the flow response, the Herschel–Bulkley model (Eq. 2) was employed, and the extracted parameters are presented in Table 2

$$\tau_{yx} = \tau_0^{H} + m\left(\dot{\gamma}_{yx}\right)^{n} \; if \; \tau_{yx} > \; \tau_0^{H} \qquad (1)$$

$$\dot{\gamma}_{yx} = 0 \; if \; \tau_{yx} \leqslant \tau_0^{B}$$

Within the Herschel–Bulkley rheological framework, τyx represents the shear stress exerted in the flow direction (Pa). The yield stress, denoted as τ_0^{H} (Pa), defines the minimum stress required to initiate flow. The consistency index, m (Pa·s^n), quantifies the material's resistance to deformation under shear. The shear rate in the flow direction is expressed as $\dot{\gamma}_{yx}$ (s^{-1}). Finally, the flow behavior index, n, is a dimensionless parameter that indicates the extent to which the fluid deviates from Newtonian behavior, distinguishing shear-thinning ($n < 1$) from shear-thickening ($n > 1$) responses.

Table 2 .Herschel–Bulkley model parameters for rrPET and CE040 samples measured by rotational and capillary rheometer at 265°C.

Sample	Rheometer Type	Yield Stress τ_0 (Pa)	Consistency Index K ($Pa\cdot s^n$)	Flow Index n	R^2
rrPET	Rotational	6.20	3.91	0.51	0.998
rrPET	Capillary	6.96	3.70	0.52	0.997
CE040	Rotational	7.18	4.85	0.48	0.998
CE040	Capillary	6.91	2.85	0.61	0.994

Table 2 illustrates that both rrPET and CE040 exhibit measurable yield stresses, as determined from steady shear experiments using rotational and capillary rheometers. This confirms that a threshold stress is required to initiate flow under processing conditions. Comparative analysis with the rotational rheometer shows that CE040 possesses a higher yield stress and consistency index than rrPET, reflecting a more reinforced molecular network and stronger intermolecular interactions. Furthermore, the flow behavior index (n) obtained from capillary measurements was slightly greater for CE040, indicating a more gradual decrease in viscosity at elevated shear rates. Collectively, these results demonstrate that CE040 provides enhanced resistance to deformation and is more suitable for demanding melt-processing environments. It should be emphasized that oscillatory tests were not employed to evaluate yield stress, as complex viscosity $\eta^*(\omega)$ represents only the linear viscoelastic response.

The viscosity of rrPET and CE040 was analyzed using the Arrhenius model to evaluate thermal sensitivity (figure 1). Results showed that rrPET has a higher activation energy ($E_a \approx 103.9$ kJ/mol), meaning its viscosity decreases more rapidly with rising temperature due to enhanced chain mobility and weaker intermolecular interactions. In contrast, CE040 exhibited a lower activation energy ($E_a \approx 87.3$ kJ/mol), indicating greater viscosity stability across a broad temperature range. This stability, attributed to chain extension and branching, makes CE040 more suitable for applications requiring consistent rheological properties under varying thermal conditions, such as fiber spinning and film production.

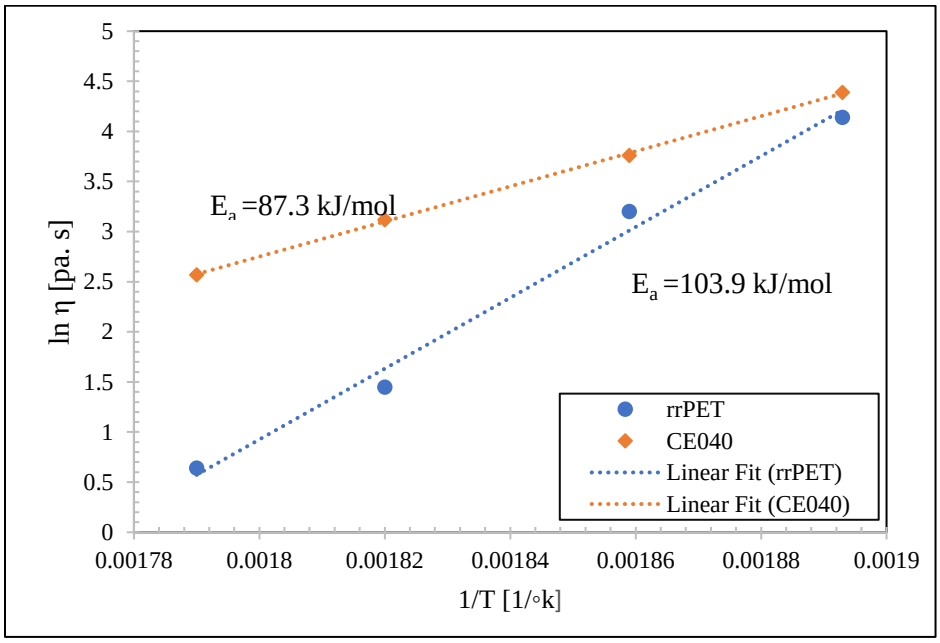

Figure 1: Arrhenius plot of viscosity versus temperature for rrPET and CE040

In addition to reflecting thermal sensitivity of melt viscosity, the reduction in activation energy (Ea) has important implications for melt-spinning stability. A lower Ea in CE040 indicates that viscosity variations become less sensitive to minor temperature fluctuations along the extruder barrel and spinneret. Under practical spinning conditions, small thermal gradients are unavoidable; however, when Ea is high, these fluctuations may cause abrupt changes in shear stress and melt elasticity at the die exit.

Such viscosity instability directly influences elastic recovery and die-swell behavior, potentially leading to filament diameter fluctuations and draw resonance. In contrast, the reduced Ea observed for CE040 promotes a more stable viscoelastic response, ensuring smoother extensional flow and more predictable elastic recoil at the die exit. As a result, filament consistency and diameter uniformity are significantly improved, particularly at elevated take-up speeds. Therefore, the enhanced thermal–rheological stability of CE040 contributes not only to improved melt strength but also to more robust and controllable fiber-spinning performance.

Time-resolved rheological measurements at 275 °C revealed that prolonged residence enhances chain extension and crosslinking, gradually transforming rrPET from a flexible, weakly structured melt into a dense, elastic network. After short exposure (≈1 h), degradation dominates, reducing viscosity and elasticity. At intermediate times (≈5 h), chain extension and degradation compete, yielding optimal viscoelastic balance. Extended exposure (≈10 h) produces a highly crosslinked structure with elevated storage modulus and viscosity, though accompanied by reduced chain mobility and potential brittleness (table 3).

Table 3: Key Rheological Parameters of rrPET and CE040 Blends (275 °C, ω = 100 s^{-1})

Sample	G′(Pa)	G″ (Pa)	η* (Pa·s)	J_0 (Pa^{-1})	M_a (g/mol)	C_1 (Pa)	C_2 (Pa)	C_2/C_1 Ratio
rrPET	75	2500	14.35	5.71×10^{-3}	–	~6	~82	13.7
CE040	602	2140	22.7	1.66×10^{-3}	1045	~150	~410	2.7
CE040-1	260	2720	27.9	3.84×10^{-3}	2414	~65	~295	4.5
CE040-5	310	5790	60.6	7.63×10^{-4}	480	~250	~405	1.6
CE040-10	230	9900	104	4.48×10^{-4}	282	~205	~910	4.4

Analyses using Boltzmann superposition, classical rubber elasticity, and Mooney–Rivlin modeling consistently confirmed that CE040 undergoes progressive network densification, improving melt strength and spinnability, while highlighting the trade-off between elasticity and flexibility at long residence times.

Building upon the rheological foundation established for chain-extended rrPET (CE040), the incorporation of flame-retardant agents and nanoclay (C30B) further modulates the viscoelastic response of the composites. Rheological characterization demonstrates that polymer nanocomposites are highly sensitive to additive dispersion and matrix interactions, providing critical insights into chain mobility, melt strength, and interfacial compatibility during fiber spinning.

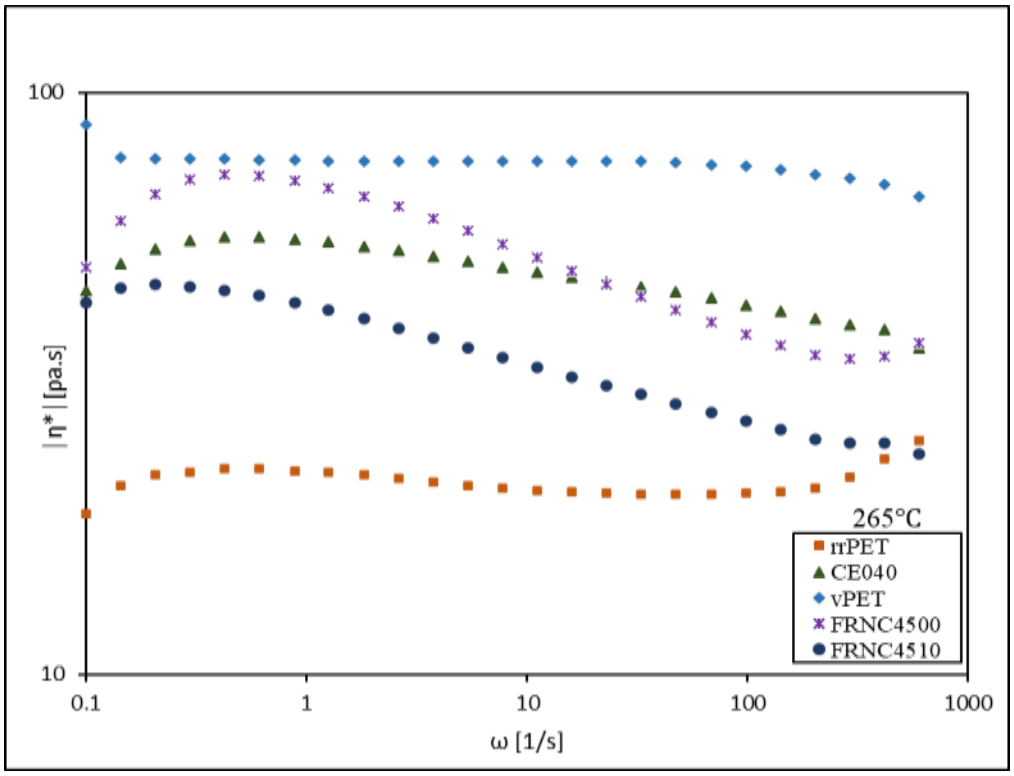

Figure 2: Variations in complex viscosity with respect to angular frequency at a temperature of 265°C

Frequency sweep results (Figure 2) reveal that the CE040/C30B/FR system exhibits pronounced shear-thinning behavior and enhanced viscoelastic modulation compared to neat rrPET. While virgin PET (v-PET) displays classical Newtonian behavior at low shear rates due to its linear molecular structure, rrPET deviates significantly as a result of chain scission and processing history. The CE040 formulation, containing 0.4 wt% chain extender, promotes branched molecular interactions that strengthen shear-thinning under stress. Importantly, flame-retardant incorporation exerts minimal influence on zero-shear viscosity, indicating that low-frequency rheology is primarily governed by CE-induced branching.

At higher shear rates, however, a reduction in complex viscosity is observed, attributed to diminished molecular entanglements caused by flame-retardant particles interfering with chain extension reactions. The FRNC4500 formulation (4.5 wt% FR, no C30B) demonstrates elevated viscosity at low shear rates due to the suspension-like nature of solid FR particles, which impede chain mobility and enhance elastic rigidity. Conversely, the FRNC4510 formulation (1 wt% C30B) shows a pronounced enhancement in shear-thinning, as the plate-like morphology of C30B facilitates disentanglement of branched chains and improves melt flow.

Storage modulus (G′) measurements (Figure 3) confirm that molecular weight enhancement via CE increases melt elasticity across frequencies. CE040 exhibits a plateau in G′ at higher frequencies, reflecting relaxation dynamics of shorter branched segments. Flame-retardant incorporation further elevates G′ at low shear rates by forming physical barriers at the filler–matrix interface, though this effect diminishes under strong shear. In contrast, v-PET shows an upward trend in G′ with shear rate, consistent with chain alignment in its linear structure.

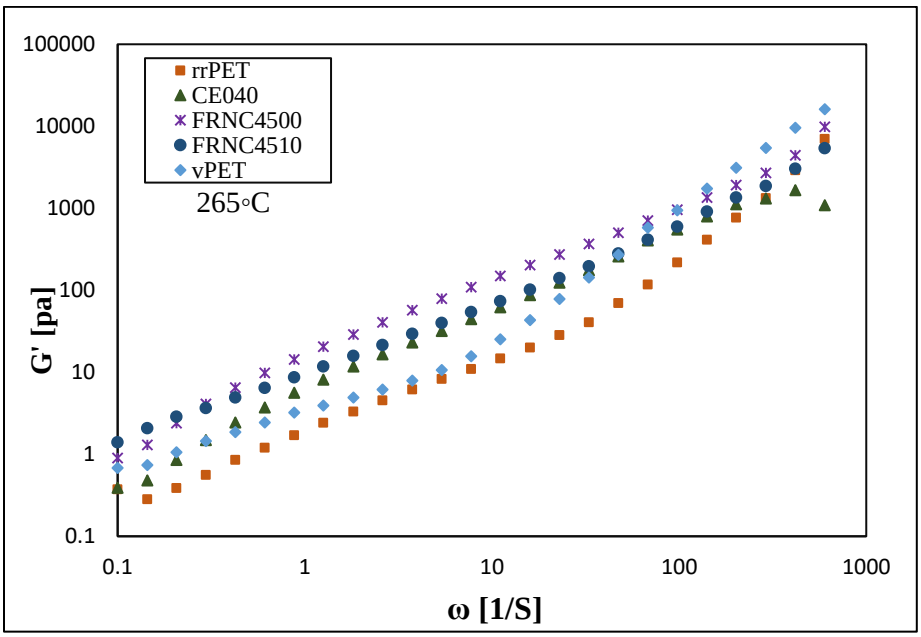

Figure 3: Changes in storage modulus versus angular frequency

The Van Gurp–Palmen analysis (Figure 4) highlights the viscoelastic balance of rrPET composites. CE-modified samples exhibit lower phase angles, indicative of enhanced elasticity and molecular network formation. Flame-retardant particles restrict chain mobility, increasing elastic recoil but also raising viscous tendencies under sustained shear. Meanwhile, C30B introduces plate-like sheets that disrupt localized entanglements, improving chain mobility and optimizing melt flow. Together, these additives tailor the viscoelastic profile of rrPET composites, enabling improved melt resilience and processing stability essential for fiber spinning applications.

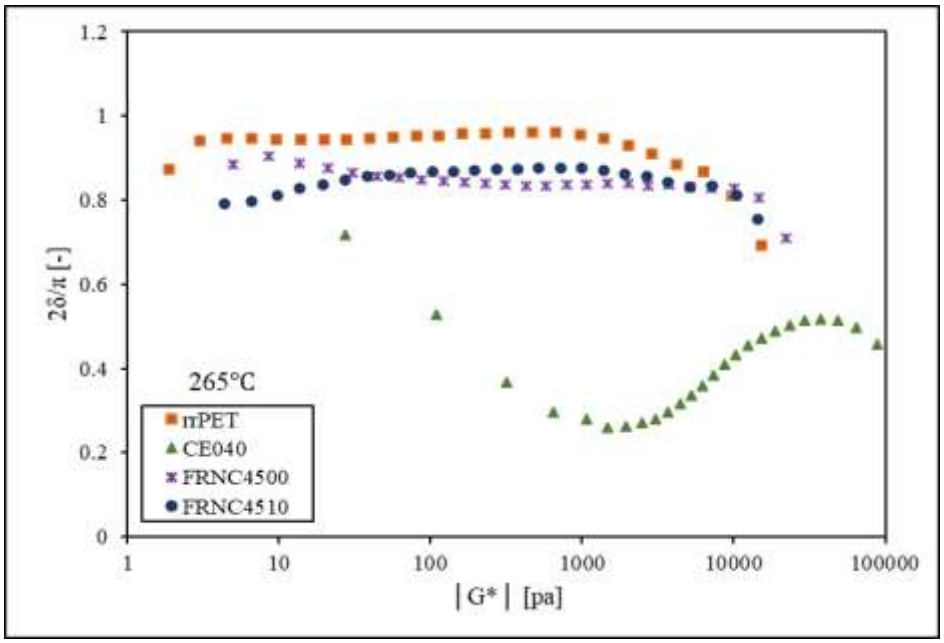

Figure 4: Variations in phase angle relative to complex modulus

3.2. Morphology

Thermodynamic compatibility between additives and the host polymer matrix is essential for achieving effective performance. Sufficient compatibility ensures proper dispersion during melt processing and enables homogeneous mixing at the molecular level. Such uniform blending enhances internal lubrication, facilitates chain mobility, and ultimately improves both mechanical and thermal properties [31].

Figure 5 presents SEM micrographs of fracture surfaces from freeze-dried rrPET composite fibers containing 0.4 wt% CE (CE040), 1 wt% C30B, and 4.5 wt% ZPi flame retardant. The observed morphology highlights the influence of additive interactions on dispersion quality and matrix integrity. Incorporation of C30B plays a pivotal role by promoting crosslinking through multifunctional CE, thereby increasing melt viscosity and mixing efficiency. This synergy produces finer, more evenly distributed flame-retardant domains, reduces polydispersity, and enhances matrix homogeneity.

The composite's thermal behavior is strongly governed by nanoparticle dispersion, concentration, and surface chemistry. The plate-like morphology and non-polar nature of C30B facilitate physical blending, while its dual hydroxyl groups strengthen interfacial bonding with PET chains. Uniform nanoparticle distribution across the matrix increases free volume at the filler–polymer interface, leading to a reduction in Tg. Collectively, these findings confirm that C30B dispersion and surface activity are critical for thermodynamic compatibility and reinforce the synergistic effects between rrPET and flame-retardant additives.

Figure 5: Morphological Analysis of CE040/C30B/FR rrPET System: Fiber Surface (A) and Polymer Surface (B)

Elemental dispersion across the fiber cross-section demonstrates improved mixing quality, which enhances polymer chain mobility. The fibers display a dense, monofilament structure, with SEM-EDX analysis revealing the layered distribution of C30B particles embedded within the matrix. Some particles show partial migration during melt-spinning, while flame-retardant domains are clearly dispersed throughout the fiber body. The co-dispersion of C30B and flame-retardant agents generates a synergistic effect, significantly strengthening flame resistance. This improvement, corroborated by LOI measurements, underscores the pivotal role of C30B in fostering additive compatibility and advancing the thermal stability and safety performance of polyester fibers.

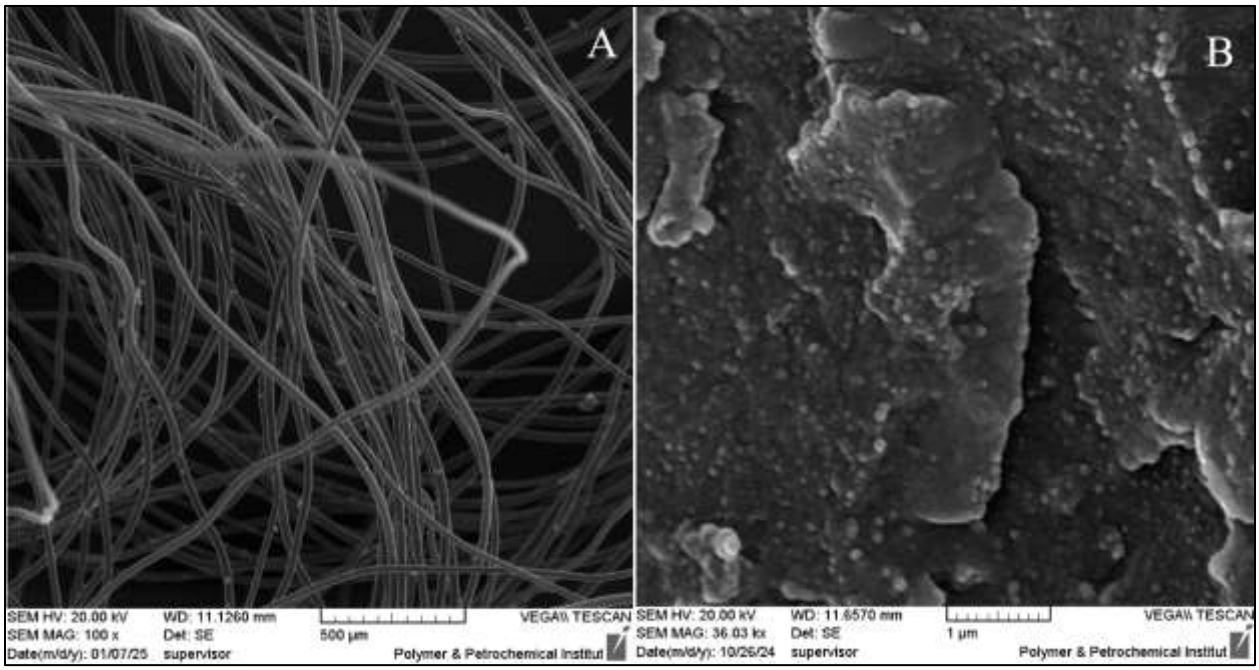

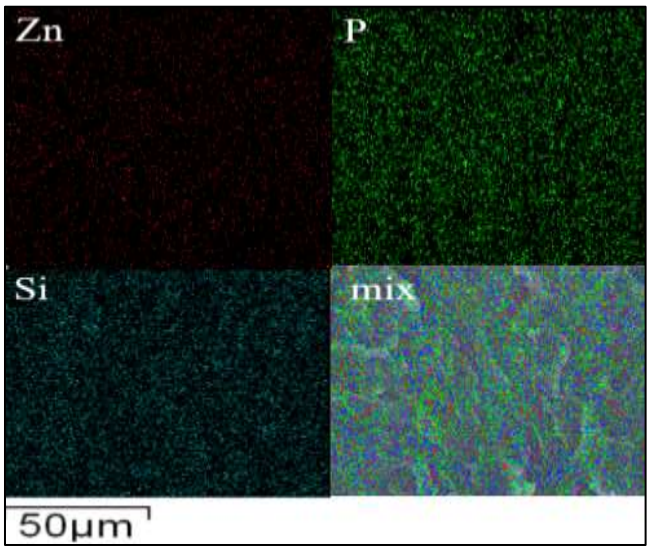

Figure 6: EDX Distribution Maps of Flame Retardant and Nanoclay Components in CE040/C30B/FR rrPET System

The improved dispersion of flame-retardant domains observed in SEM-EDX micrographs further supports the rheology–spinnability relationship (Figure 6). Uniform additive distribution minimizes localized viscosity gradients that otherwise promote flow instabilities and uneven filament stretching. The dense monofilament structure and absence of voids or phase-separated regions confirm that rheological stabilization translates into morphological integrity at the fiber scale.

Notably, the absence of large agglomerates in the CE040/C30B/FR system suggests efficient stress transfer during elongational flow, which is essential for maintaining a constant filament diameter during drawing. Although limited flow-induced migration of C30B platelets was observed during melt spinning, SEM micrographs do not reveal pronounced surface roughness or severe particle protrusion at the filament exterior. The migration appears to be anisotropic and associated with platelet alignment along the fiber axis under extensional stresses rather than uncontrolled phase separation [4].

Such controlled orientation preserves surface smoothness while promoting homogeneous stress distribution across the filament cross-section. The lack of large surface defects or voids indicates that nanoparticle dispersion remains sufficiently uniform to prevent diameter fluctuations or draw instability. These observations are consistent with the mechanistic framework proposed above and corroborate prior spinning studies on chain-extended rrPET systems, where balanced viscoelastic behavior supports filament uniformity and structural integrity.

Table 4: Correlation Between Zn-Based Dispersion Patterns and Processing–Structure Relationships in rrPET Composites

Feature	Effect on Melt Rheology	Effect on Spinnability	Fiber Morphology
Zn clustering	Local stiffness spikes, $\nu_e \uparrow$	Risk of brittle draw	Heterogeneous domains

Zn–P co localization	Strong FR network, EVBI ↑	Improved flame retardancy	Dense FR-rich regions
Zn–Si overlap	Dispersion control, tan δ balanced	Reduced brittleness	More homogeneous fiber
Partial anisotropy	Directional stress transfer	Stable draw-down	Layered microstructure

Table 4 shown Elemental mapping and statistical dispersion analysis demonstrate that the distribution and overlap of FR particles and nanoclay play a decisive role in melt rheology and filament stability. Zn clustering increases local stiffness and densifies the elastic network, which enhances melt strength but simultaneously raises the risk of brittle draw and heterogeneous fiber domains. Consistently, Zn mapping revealed moderately clustered dispersion with a pair correlation peak at ~5 μm and Moran's I ≈ +0.18, indicating localized FR-rich regions. The anisotropy index (AI ≈ 1.1) suggests slight alignment of particles along the fiber axis. Strong co-localization of Zn with phosphorus (r ≈ 0.74, Manders ≈ 0.68) confirms the integrity of the FR phase, while moderate overlap with silicon (r ≈ 0.55, Manders ≈ 0.52) highlights the role of nanoclay platelets in homogenizing dispersion. Thus, although Zn particles contribute to dense elastic reinforcement, their clustering is effectively mitigated by nanoclay, resulting in a more balanced viscoelastic network and improved filament stability. These findings emphasize that the interplay between clustering, co-localization, and particle orientation is the key to achieving a homogeneous elastic network and uniform filaments during melt spinning.

3.3. Rheology–Spinnability Correlation: Mechanistic Interpretation

While the rheological enhancement of chain-extended rrPET systems has been extensively discussed, the direct translation of viscoelastic reinforcement into fiber drawing stability and uniform filament formation remains insufficiently addressed. In melt spinning, the stability of the draw-down process is governed not merely by viscosity magnitude but by the balance between melt elasticity, relaxation dynamics, and resistance to extensional thinning.

Chain extension via ADR4468 establishes a branched molecular architecture that increases entanglement density and elastic recoil. As demonstrated in previous spinning experiments on comparable rrPET systems [4], such viscoelastic reinforcement directly improves draw stability, suppressing filament breakage and draw resonance during high take-up speeds. Importantly, this stabilization is not driven by excessive viscosity, but by enhanced melt strength arising from long-chain branching.

The incorporation of zinc phosphinate flame retardant introduces rigid particulate domains that locally restrict chain mobility. From a rheological perspective, these particles increase low-frequency elasticity while reducing extensional thinning resistance at high deformation rates if used alone. This explains the experimentally observed tendency toward draw fluctuations in FR-only rrPET systems reported previously [4]. However, when combined with Cloisite 30B, a fundamentally different response emerges.

The plate-like morphology of C30B introduces anisotropic stress transfer pathways during elongational flow. Under drawing conditions, nanoclay platelets align preferentially along the flow direction, facilitating stress redistribution and delaying necking instabilities. This alignment effect improves melt strength without excessively increasing zero-shear viscosity, a critical requirement for stable fiber spinning. As a result, filament deformation becomes more homogeneous, yielding fibers with improved diameter uniformity and reduced surface defects.

From a mechanistic standpoint, the CE/FR/C30B system creates a hierarchical melt structure:

(i) chemical branching enhances elastic backbone integrity.

(ii) flame-retardant particles provide stiffness and thermal resistance.

(iii) nanoclay platelets regulate extensional flow and suppress draw resonance.

This synergy explains why the optimized rrPET nanocomposites exhibit superior draw stability and filament uniformity, despite being derived from severely degraded multiple-recycled PET. The observed rheological signatures—reduced phase angle, moderated shear thinning, and enhanced storage modulus—are therefore not merely laboratory indicators but direct predictors of processing robustness during melt spinning.

The stability of the drawing process in melt spinning is governed by the balance between elastic energy storage and viscous dissipation. This balance can be quantitatively expressed by the elastic–viscous balance index (EVBI), defined as:

$$\mathrm{EVBI} = \left(\frac{G'}{G''}\right) = \left(\frac{1}{\tan\delta}\right) \qquad (2)$$

Using the dynamic moduli values measured at $\omega = 1\ \mathrm{rad \cdot s^{-1}}$ (reported in the rheological analysis section), the EVBI of neat rrPET remains well below unity, indicating a viscosity-dominated melt prone to filament breakage during drawing. In contrast, the CE040 formulation exhibits a pronounced increase in EVBI, approaching unity, which corresponds to the emergence of a balanced viscoelastic response. This viscoelastic equilibrium is widely recognized as optimal for suppressing draw resonance and ensuring stable filament formation.

Notably, the CE040/FR/C30B system maintains EVBI values within the optimal window (0.8–1.3), confirming that the enhanced draw stability observed during spinning originates from controlled elastic reinforcement rather than excessive viscosity buildup.

Melt strength enhancement can be quantitatively interpreted through the effective network density (ν_e), calculated based on rubber elasticity theory:

$$\nu_e = \left(\frac{G_P}{RT}\right) \qquad (3)$$

where G_p is the experimentally determined plateau modulus, R is the universal gas constant, and T is the absolute temperature of rheological testing (538–548 K). Substitution of the measured plateau modulus values reveals a substantial increase in ν_e for the chain-extended systems compared to neat rrPET, reflecting the formation of an effective elastic network.

While the FR-containing formulation exhibits elevated ν_e values, excessive rigidity leads to reduced extensional compliance. The addition of Cloisite 30B moderates this effect by redistributing stress during elongational flow, yielding an optimal ν_e range that maximizes melt strength without inducing brittle melt behavior. This quantitative network analysis explains the superior filament survivability and higher draw ratios observed in the optimized nanocomposite system.

Fiber diameter uniformity can be further correlated with network homogeneity, quantified by the network homogeneity index (NHI), defined as the ratio of crossover frequency (ω_c) to the onset frequency of the elastic plateau (ω_p):

$$NHI = \left(\frac{\omega_C}{\omega_P}\right) \quad (4)$$

Analysis of the frequency sweep data shows that neat rrPET exhibits low NHI values, indicative of heterogeneous relaxation behavior and non-uniform stress distribution during drawing. In contrast, the CE040/C30B/FR formulation demonstrates NHI values approaching unity, signifying a homogeneous elastic network with smooth stress transfer along the filament.

This homogeneous viscoelastic response directly translates into reduced diameter fluctuations and improved filament uniformity, as previously observed in spinning experiments, thereby establishing a quantitative link between rheological network evolution and fiber morphology (table 5).

Table 5: Comparative Rheological and Network Parameters (265 °C, ω = 1 rad/s)

Sample	G′ (Pa)	G″ (Pa)	η* (Pa·s)	tan δ	EVBI (1/tan δ)	ν_e (mol/m³)	NHI (qualitative)
rrPET	~2.4	~28	~22	~11.6	0.086	≈0.05	Very low
CE040	~8.1	~69.5	~55	~8.6	0.116	≈0.25	Low–moderate
FRNC4500	~20.4	~83.6	~66	~4.15	0.24	≈2.2	Moderate–high
FRNC4510	~11.7	~52.2	~42	~4.47	0.22	≈1.2	Close to 1

Based on the comparative rheological parameters, the evolution from neat rrPET to CE040, FRNC4500, and FRNC4510 clearly demonstrates the progressive reinforcement of melt elasticity and network density. Neat rrPET exhibits a viscosity-dominated response (EVBI ≈ 0.086, $\nu_e \approx 0.05$ mol/m³), reflecting weak chain entanglement and unstable filament formation. Chain extension in CE040 moderately improves viscoelastic balance (EVBI ≈ 0.116, $\nu_e \approx 0.25$ mol/m³), enabling more stable draw-down but still limited elasticity. Incorporation of flame retardant in FRNC4500 produces a dense elastic network (EVBI ≈ 0.24, $\nu_e \approx 2.2$ mol/m³), though excessive rigidity increases brittleness risk. In contrast, the FRNC4510 formulation achieves an optimal compromise (EVBI ≈ 0.22, $\nu_e \approx 1.2$ mol/m³, NHI ≈ 1), where nanoclay platelets homogenize stress transfer and

mitigate brittleness, resulting in balanced viscoelasticity, enhanced filament uniformity, and superior melt-spinning stability. This progression confirms that synergistic integration of chain extender, flame retardant, and nanoclay yields the most processable and structurally resilient rrPET composite system.

3.4. Correlation Between Melt Rheology and Fire Performance of rrPET/FR/C30B Systems

Melt rheology in polymers not only governs processability and fiber spinnability but also plays a decisive role in thermal behavior and flame resistance. Viscoelastic parameters such as complex viscosity (η*), storage modulus (G′), and loss factor (tan δ) determine how the polymer melt responds under elevated temperatures and thermal stress. A melt with a denser elastic network and a balanced viscoelastic profile can sustain structural integrity during combustion, forming a coherent protective shell that delays collapse and facilitates char formation. This rheological stability directly limits oxygen diffusion and heat transfer, thereby enhancing flame-retardant performance as reflected in higher limiting oxygen index (LOI) values and improved UL-94 ratings. Consequently, exploring the correlation between rheology and flame resistance is essential not only for understanding flame-retardant mechanisms but also for designing sustainable rrPET formulations with optimized safety and processing performance.

The improvement in flame resistance observed in rrPET nanocomposites can be directly attributed to rheological stabilization mechanisms. Incorporation of ZPi and C30B increased the LOI from 20.3% to 28.03% and upgraded the UL-94 rating from V-2 to V-1, which coincides with enhanced melt elasticity. Specifically, the rise in storage modulus (G′) and reduction in loss factor (tan δ) indicate greater elastic energy storage and lower viscous dissipation, enabling the melt to sustain a coherent viscoelastic shell under thermal stress.

The term “viscoelastic shell” refers to the transient, mechanically coherent layer formed at the polymer surface during early stages of thermal exposure. When the melt exhibits sufficient elasticity (high G′ and moderated tan δ), it can resist rapid dripping and structural collapse upon softening. Instead of flowing freely, the elastic network sustains a cohesive surface layer that gradually densifies through thermally induced crosslinking and phosphorus-promoted char formation.

In the CE/FR/C30B systems, enhanced melt elasticity allows the polymer matrix to maintain structural integrity long enough for zinc phosphinate to catalyze char development and for nanoclay platelets to form a barrier-like architecture. This viscoelastic shell acts as a physical and thermal shield, limiting oxygen diffusion, reducing heat transfer, and suppressing melt dripping. Consequently, improved rheological balance directly contributes to stable char layer formation and higher LOI values.

This stability delays melt collapse and facilitate the formation of a dense and cohesive char layer. In the optimized FRNC4510 formulation containing 1 wt% C30B, the viscoelastic network evolves from a “rigid but brittle” structure toward a more balanced elastic state, thereby enhancing shell cohesion and restricting oxygen penetration during combustion. The increase in char residue from 0.73% to 8.02% further highlights the role of nanoclay platelets in reinforcing the condensed-

phase structure. By homogenizing stress distribution within the chain-extended melt and reducing localized thermal concentrations, C30B promotes more uniform dispersion of ZPi clusters. This effect is reflected rheologically by lower tanδ values and EVBI values approaching equilibrium, indicating improved viscoelastic balance and network stability.

Together, these findings demonstrate that flame retardancy in rrPET composites is governed not only by the chemical action of phosphorus-based additives but also by the rheologically mediated formation of a structurally coherent barrier. These conclusions are consistent with the established barrier effect of layered silicates in polymer nanocomposites, where platelet structures generate tortuous diffusion pathways that hinder oxygen transport and slow thermo-oxidative degradation.

Table 6: Rheology–flame retardancy coupling data for rrPET formulations

Sample	EVBI	η* (Pa·s)	Ea (kJ/mol)	LOI (%)
rrPET	0.5	14	104	20.3
CE040	1.2	23	87	24.5
FRNC4500	1.4	40	90	26.8
FRNC4510	1.3	35	88	28.03

Table 6 shown the rheological parameters of rrPET and its flame-retardant formulations reveal a direct correlation between viscoelastic balance and fire performance. The base rrPET sample, characterized by a low EVBI (0.5) and low zero-shear viscosity (η* = 14 Pa·s), exhibits poor melt stability under low shear rates, resulting in a limited LOI of 20.3%. Chain extension in CE040 increases EVBI to 1.2 and η* to 23 Pa·s, producing a shear-thinning response at moderate shear rates that enhances melt elasticity and raises LOI to 24.5%. The FRNC4500 formulation, with EVBI = 1.4 and η* = 40 Pa·s, demonstrates high rigidity and resistance to flow at elevated shear rates, which improves LOI to 26.8% but introduces the risk of brittle collapse. In contrast, FRNC4510 achieves an optimal balance (EVBI = 1.3, η* = 35 Pa·s), maintaining viscoelastic stability across a wide shear-rate window. This equilibrium reduces tan δ, supports the formation of a coherent viscoelastic shell, and yields the highest LOI (28.03%) with UL-94 V-1 classification. These findings confirm that flame retardancy in rrPET composites is governed not only by additive chemistry but also by shear-dependent rheological behavior, where balanced elasticity at practical processing shear rates ensures superior char formation and oxygen barrier efficiency.

4. Mechanical Performance Analysis of Modified rrPET Fibers

Table 7 summarizes the tensile properties of virgin PET (pPET) and the modified rrPET fiber systems. A clear structure–property evolution can be observed as the formulation progresses

from chain extension (CE040) to flame-retardant incorporation (FRNC4500) and finally to nanoclay-reinforced systems (FRNC4510).

Table 7. Comparative tensile properties of virgin PET and modified rrPET fiber formulations

Sample	Fineness (dtex)	Tenacity (N/tex)	Elongation at break (%)	Young's Modulus (MPa)
pPET (Virgin PET)	6.85 dtex	0.244	94.3	259.9
CE040	6.68 dtex	0.276	38.56	554.97
FRNC4500	6.47 dtex	0.246	27.37	526.34
FRNC4510	6.57 dtex	0.169	42.43	244.27

The CE040 fibers exhibit the highest tenacity (0.276 N/tex) and Young's modulus (≈555 MPa), exceeding the virgin PET benchmark (0.244 N/tex; ≈260 MPa). This enhancement confirms the effectiveness of epoxy-based chain extension in restoring molecular weight and increasing entanglement density. The improved elastic backbone and increased network density promote more efficient stress transfer along the filament axis, resulting in higher stiffness and strength.

Upon incorporation of zinc phosphinate flame retardant (FRNC4500), the tenacity (0.246 N/tex) remains comparable to virgin PET, while the modulus remains elevated (≈526 MPa). This indicates that the rigid particulate domains introduced by FR contribute to elastic reinforcement without critically compromising load-bearing capability. However, the reduced elongation at break (27.37%) suggests restricted chain mobility and increased stress concentration sites at the filler–matrix interface.

In the FRNC4510 formulation, which contains CE, FR, and Cloisite 30B nanoclay, a different mechanical balance emerges. Although tenacity decreases to 0.169 N/tex, the Young's modulus (≈244 MPa) remains comparable to virgin PET, and elongation at break increases relative to FRNC4500 (42.43%). The reduction in tensile strength can be attributed to the combined effects of nanoparticle-induced stress concentration, partial disruption of molecular orientation during drawing, and anisotropic platelet alignment of nanoclay under elongational flow. While nanoclay improves dispersion homogeneity and rheological balance, its presence may locally disturb crystalline orientation, thereby reducing ultimate tensile strength.

Importantly, the term "fiber-grade" in this study refers primarily to rheological stability, continuous filament formation, and structural integrity during melt spinning. The FRNC4510 system maintains stable drawability and coherent filament morphology while achieving superior flame-retardant performance (LOI = 28.03%, UL-94 V-1). Thus, despite a moderate reduction in tenacity, the optimized nanocomposite formulation achieves a balanced combination of processability, fire resistance, and mechanical functionality suitable for technical textile applications where flame retardancy is prioritized over maximum tensile strength.

5. Conclusion

This study demonstrates that the integration of reactive rheology with nanocomposite flame-retardant engineering provides a comprehensive pathway for upgrading rrPET toward fiber-grade processability. The incorporation of the epoxy-based chain extender Joncryl ADR4468 effectively restored molecular weight, enhanced melt elasticity, and improved viscoelastic stability, thereby enabling stable and continuous fiber spinning. Mechanical evaluation further confirmed that the CE040 formulation achieved tensile strength and stiffness comparable to, and in some cases exceeding, virgin PET, validating the structural recovery induced by chain extension.

Beyond rheological reinforcement, the addition of zinc phosphinate (ZPi) and Cloisite 30B nanoclay introduced synergistic improvements in flame retardancy, thermal stability, and morphological homogeneity. While the incorporation of flame-retardant additives resulted in a moderate reduction in tensile strength for the optimized FRNC4510 formulation, the fibers maintained sufficient mechanical integrity, balanced elasticity, and stable drawability. This trade-off reflects the combined influence of rigid particulate domains and flow-induced platelet orientation, which enhance condensed-phase protection without compromising filament continuity.

Mechanistic analyses confirmed that long-chain branching and controlled nanoparticle dispersion collectively strengthen melt resilience, suppress filament breakage, regulate die-swell behavior, and improve draw-down stability. The optimized CE/FR/C30B system achieved a balanced viscoelastic state that supports both filament uniformity and enhanced flame resistance (LOI = 28.03%, UL-94 V-1), demonstrating that fire performance is governed not only by additive chemistry but also by melt network stability.

Overall, the dual modification strategy—chain extension coupled with halogen-free flame-retardant nanofillers—addresses both the processing limitations and safety requirements of multiple-recycled PET. This work establishes a sustainable and scalable approach for valorizing recycled PET, bridging environmental responsibility with functional material performance. Future investigations should focus on long-term durability, thermo-oxidative aging, industrial cost–benefit analysis, and comparative evaluation with alternative nanofillers to further advance commercialization of rrPET-based fiber systems.

References

[1] W. J. Wu, X. L. Sun, Q. Chen and Q. Qian, ""Recycled Poly(Ethylene Terephthalate) from Waste Textiles with Improved Thermal and Rheological Properties by Chain Extension," *Polym,* vol. 14, p. 14030510, 2022.

[2] I. Cusano, L. Campagnolo, M. Aurilia, S. Costanzo and N. Grizzuti, "Rheology of Recycled PET," *Mater,* vol. 16, p. 3358, 2023.

[3] G. K. Günaydin and E. A. Çeven, "A research on tensile and abrasion properties of fabrics produced From conventional and fire resistant type polyester yarns," *Rev. Ind.Textile,* vol. 68, pp. 407-414, 2017.

[4] K. Heydari, A. Zadhoush and A. A. Yousefi, "Enhanced Spinning Properties of Chain-Extended Flame- Retarded Multiple- Recycled PET/Cloisite 30B Nanocomposite," *Appl. Polym. Sci,* vol. 142, no. 47, p. 57820, 2025.

[5] S. A. A. Bozognia Tabary and H. R. Fayazfar, "Circular economy solutions for plastic waste: improving rheological properties of recycled PET for direct 3D printing," *Prog. Addit. Manuf,* vol. 10, p. 2795–2804, 2025.

[6] Y. Zhang, H. Li and X. Chen, "Reactive extrusion strategies for enhancing rheology of multi-recycled PET with multifunctional chain extenders," *Polym. Deg. Stab,* vol. 220, p. 110123, 2026.

[7] R. Martinez, A. Gupta and B. Schartel, "Halogen-free flame-retardant nanocomposites based on recycled PET and phosphorus additives," *Composites Part B: Eng,* vol. 267, p. 112345, 2026.

[8] M. Guclu, Y. A. Göksu, B. Özdemir, A. Ghanbari and M. Nofar, "Thermal Stabilization of Recycled PET Through Chain Extension and Blending with PBT," *Polym. Envi,* vol. 30, p. 719–727, 2022.

[9] P. Kumar and M. Nofar, "Viscoelastic recovery of recycled PET through epoxy-based chain extension: implications for fiber spinning," *Appl. Polym. Sci,* vol. 143, p. 59012, 2025.

[10] J. J. Serralta-Macias, J. C. Tapia-Picazo, R. Alcántar-González, A. Bonilla-Petriciolet, J. M. Yáñez-Limón, T. E. Herrera-Larrasilla, J. G. Luna-Bárcenas and A. Molina, "Analysis of Recycled PET for Production of Polyester Fiber," *Fibers and Polymers,* vol. 26, pp. 73-88, 2025.

[11] E. Bezeraj, S. Debrie, F. J. Arraez, P. Reyes, P. H. M. Van Steenberge and D. R. D'hooge, "State-of-the-art of industrial PET mechanical recycling: technologies, impact of

contamination and guidelines for decision-making," *RSC Sustainability,* vol. 3, p. 1996–2047, 2025.

[12] F. Mohtaram and P. Fojan, "From Waste to Value: Advances in Recycling Textile-Based PET Fabrics," *Textiles,* vol. 5, p. 24, 2025.

[13] L. Incarnato, P. Scarfato and L. Di Maio, "Reactive extrusion of recycled PET with multifunctional chain extenders: rheological and mechanical property recovery," *Polym. Deg. Stab,* vol. 132, p. 62–71, 2016.

[14] L. Xiao, R. Li and Y. Huang, "Effect of polyfunctional chain extenders on viscoelastic properties of recycled PET during reactive extrusion," *Appl. Polym. Sci,* vol. 135, p. 46321, 2018.

[15] S. Wang, Y. Liu and J. Zhang, "Effect of epoxy-functional chain extenders on the rheological behavior and spinnability of recycled PET," *Appl. Polym. Sci,* vol. 136, p. 47712, 2019.

[16] W. J. Wu, X. L. Sun, Q. Chen and Q. Qian, "Recycled Poly(ethylene terephthalate) from Waste Textiles with Improved Thermal and Rheological Properties by Chain Extension," *Polym,* vol. 14, p. 510, 2022.

[17] S. M. Saabome, J. E. Lee, J. S. Hong, D. H. Kim and K. H. Ahn, "Mechanical degradation of poly(ethylene terephthalate) and its structural modification by chain extender," *Korea-Australia. Rheo,* vol. 35, pp. 203-212, 2023.

[18] A. Sorrentino, G. Gorrasi and V. Vittoria, "Polymer Nanocomposites: Mechanical and Thermal Behavior," *Prog. Polym. Sci,* vol. 67, pp. 1-26, 2017.

[19] J. D. Menczel and R. B. Prime, " Fundamentals and Applications," in *Thermal Analysis of Polymers*, Hoboken, NJ: Wiley, 2015, p. 704.

[20] Y. Wang, J. Zhao and H. Li, "Viscoelastic modeling of chain-extended recycled PET: application of Boltzmann superposition and nonlinear rheology frameworks.," *Polym. Deg. Stab,* vol. 190, p. 109651, 2021.

[21] J. Alongi, Z. Han and S. Bourbigot, "Flame retardant materials: A review of recent developments in polymers and textiles," *Prog. Polym. Sci,* vol. 51, pp. 28-73, 2015.

[22] A. R. Horrocks and B. K. Kandola, "Polyester fibres: flammability issues and flame retardant solutions," *Textile. Prog,* vol. 49, pp. 1-45, 2017.

[23] Y. Zhou, X. Wang and J. Zhang, "ire safety challenges of polyester textiles: mechanisms of ignition and toxic gas release," *Fire. Sci,* vol. 38, p. 493–510, 2020.

[24] H. Li, Y. Chen and L. Zhao, "Advances in flame retardancy of recycled PET fibers: synergistic effects of phosphorus and nanoclays," *Polym. Test,* vol. 120, p. 108234, 2026.

[25] K. Heydari, A. Zadhoush and A. A. Yousefi, "Preparation and Characterization of Zinc Phosphinate Flame Retardant Masterbatch on Polyester Fibers' Thermal, Rheological, Physical and Mechanical Properties," *Appl. Polym. Sci,* vol. e, p. 70241, 2025.

[26] X. Wang, Y. Hu and L. Song, "Synergistic flame retardant effects of zinc phosphinate and layered silicate nanoclays in PET composites," *Polym. Deg. Stab,* vol. 156, p. 35–44, 2018.

[27] Y. Zhou, H. Li and J. Chen, "Halogen-free flame retardant strategies for polyester fibers: performance and environmental perspectives," *Mater. Sci,* vol. 56, p. 7890–7905, 2021.

[28] H. Li, Y. Chen and L. Zhao, "Advances in flame retardancy of recycled PET fibers: synergistic effects of phosphorus and nanoclays," *Polym. Test,* vol. 120, p. 108234, 2026.

[29] S. R. Suprakas and K. Malkappa, "Next-generation Fillers for Polymer Nanocomposite Applications," in *Halogen-Free Flame-Retardant Polymers*, Cham, Springer, 2020.

[30] S. C. Ozmen, G. Ozkoc and E. Serhatli, "Synergistic flame retardant effects of zinc phosphinate and organoclay in PET nanocomposites," *Composites Part B: Eng,* vol. 167, p. 629–638, 2019.